Concurrent Wireless Power Transfer in the Internet of Batteryless Things: Experiment and Modeling

Ye Liu, Senior Member, IEEE, Honggang Wang, Fellow, IEEE, and Mikael Gidlund, Senior Member, IEEE

Abstract—The advancement of energy harvesting technologies, coupled with the adoption of ultra-low-power IoT devices, have enabled the emergence of the Internet of Batteryless Things (IoBT). This innovative paradigm envisions a sustainable future by employing radiative wireless power transfer (RWPT) to support battery-free IoT device operation. Despite significant progress in optimizing one-to-one RWPT, a systematic understanding of the dynamics of concurrent RWPT is still lacking. This includes addressing complex situations such as one-to-many, many-to-one, and many-to-many concurrent power transfer. These gaps hinder the scalability and practical implementation of distributed RWPT networks in real-world IoBT environments. This study addresses these challenges by conducting comprehensive experimental evaluations and developing detailed theoretical models for concurrent RWPT across all four fundamental scenarios. By leveraging state-of-the-art wireless power development kits, the novel experimental observations provide key insights into spatial power distribution. For instance, the movement of a neighboring IoT node can either double a battery-free IoT node's received power or reduce it to nearly zero. Furthermore, analytical models grounded in electromagnetic field theory, circuit principles, and wave propagation dynamics are proposed to predict and optimize RWPT performance across diverse scenarios, and are validated by MATLAB simulation. This work represents the first unified framework for concurrent RWPT, offering valuable contributions to the design of scalable, energy-efficient IoBT systems.

Index Terms—wireless power transfer, concurrent transmission, Internet of Batteryless Things, zero-energy devices, experimental study, theoretical modeling.

I. INTRODUCTION

THE rapid advancement of energy harvesting technologies [1], [2] and the proliferation of ultra-low-power devices [3]–[5] have paved the way for the Internet of Batteryless Things (IoBT) [6]–[8]. This emerging paradigm envisions a sustainable future where devices operate solely on ambient energy, eliminating the need for conventional batteries. A cornerstone of IoBT is radiative wireless power transfer (RWPT) [9]–[11], which enables devices to harvest energy wirelessly from electromagnetic waves. By supporting the uninterrupted operation of battery-free IoT devices, RWPT

Corresponding author: Honggang Wang.

Ye Liu is with the Department of Graduate Computer Science and Engineering, Katz School of Science and Health, Yeshiva University, New York, NY 10016 USA, and the Department of Computer and Electrical Engineering, Mid Sweden University, 85170 Sundsvall, Sweden (e-mail: yliu26@mail.yu.edu).

Honggang Wang is with the Department of Graduate Computer Science and Engineering, Katz School of Science and Health, Yeshiva University, New York, NY 10016 USA (e-mail: yliu26@mail.yu.edu; honggang.wang@yu.edu).

Mikael Gidlund is with the Department of Computer and Electrical Engineering, Mid Sweden University, 85170 Sundsvall, Sweden (e-mail: mikael.gidlund@miun.se).

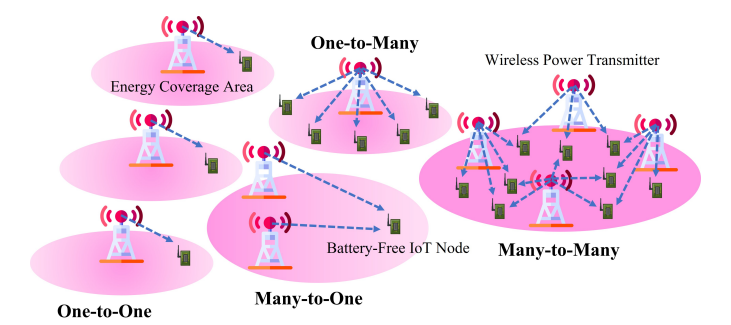


Fig. 1. The four fundamental concurrent wireless power transfer scenarios.

plays a critical role in applications such as environmental monitoring, smart agriculture, and industrial automation.

As shown in Fig. 1, four fundamental power transfer scenarios have been identified within the realm of RWPT [12]: one-to-one device, many-to-one device, one-to-many devices, and many-to-many devices. Each of these scenarios caters to distinct use cases and poses unique technical challenges. For instance, while the one-to-one scenario is foundational and widely adopted in isolated settings, the one-to-many and many-to-one concurrent RWPT enable simultaneous charging of multiple devices or the aggregation of energy from distributed sources. The many-to-many case, representing the most complex scenario, involves concurrent power exchanges between multiple transmitters and receivers, which is essential for densely populated IoBT ecosystems.

Significant advancements have been made in one-to-one RWPT research in recent years, with particular focus on optimizing energy transfer efficiency [13]–[15], ensuring spatial power distribution [16], and integrating simultaneous wireless information and power transfer (SWIPT) capabilities [17]. In parallel, researchers have explored the feasibility of reconfigurable intelligent surface (RIS)-aided one-to-one RWPT through both simulation and experimental prototypes [18], [19]. However, the literature reveals an overemphasis on single-transmitter, single-receiver scenario [20], [21], leaving more complex scenarios such as concurrent RWPT in multi-transmitter or multi-receiver situations underexplored. This has resulted in a lack of comprehensive experimental validation and robust theoretical frameworks for these scenarios.

Although some progress has been made in studying concurrent RWPT, empirical investigations into one-to-many, many-to-one, and many-to-many scenarios remain sparse [12]. In addition, existing theoretical studies on concurrent RWPT [22]–[24] are often based on simplified assumptions, neglecting

the complex interactions that occur among concurrent power transfer paths. For instance, ideal conditions such as precise time synchronization and perfect phase alignment are assumed among multiple wireless power transmitters. However, achieving tight synchronization in practical powering networks is challenging, if not infeasible. Furthermore, current studies often treat multiple battery-free IoT nodes as independent entities, ignoring the potential for energy interference among nodes. This oversimplification overlooks the nuanced interplay between concurrent power transfer paths, significantly limiting the scalability and practical deployment of wireless powered IoBT. Furthermore, the absence of a complete and generalizable model for concurrent RWPT in these complex scenarios underscores the need for further research.

This study seeks to bridge the aforementioned gaps by conducting a comprehensive experimental investigation and developing detailed models for concurrent RWPT in the IoBT. Specifically, the research addresses the following critical questions: (i) How do concurrent RWPT affect energy transfer efficiency and spatial power distribution in realworld scenarios? (ii) What are the key factors influencing the performance of one-to-one, many-to-one, one-to-many, and many-to-many concurrent RWPT? (iii) How can a unified framework be developed to accurately predict and optimize RWPT performance across all configurations? To answer these questions, the study employs a mixed-method approach combining rigorous experimental measurements with advanced analytical modeling. The experimental setup closely replicates real-world IoBT environments, incorporating key physical and environmental factors. The primary contributions of this work are summarized as follows:

- To the best of our knowledge, this research presents the first systematic experimental study and analytical modeling of concurrent RWPT across all four fundamental scenarios: one-to-one, many-to-one, one-to-many, and manyto-many. This effort provides a holistic understanding of RWPT behavior under diverse situations, paving the way for future advancements in networked RWPT.
- Unlike prior studies that often rely on idealized assumptions (such as perfect synchronization and independent operation of multiple nodes), we focus on realistic experimental evaluations. The experiments using state-of-the-art Powercast development kits explore how wireless power transmitters and receivers interact under varying conditions across different network scenarios. The experimental results reveal novel insights into the dynamics of concurrent RWPT, highlighting the influence of factors such as network density, topology, and device heterogeneity on system performance. By bridging these gaps, this work provides actionable guidelines for optimizing node deployment and system design in IoBT networks.
- Building on the experimental findings, we developed practical analytical models and validated their effectiveness through MATLAB simulations. By systematically extending these models across one-to-one, many-to-one, one-to-many, and many-to-many scenarios, we develop a unified modeling framework capable of capturing the

intricate interactions of concurrent power transfer paths. This unified framework not only accounts for real-world complexities (i.e., energy interference and imperfect synchronization), but also enables accurate performance prediction and optimization of concurrent RWPT in distributed wireless powering IoBT networks.

The remainder of this paper is structured as follows: Section II provides a summary of related work. Section III presents the experimental results, followed by the development of analytical models and validation in Section IV and Section V. Finally, Section VI concludes the study and outlines directions for future research.

II. RELATED WORK

A growing body of literature has investigated wireless power transfer and concurrent transmission, with an increasing emphasis on their integration and application in the IoBT. This section reviews related works across three key areas: modeling concurrent RWPT, experimental studies on concurrent RWPT, and concurrent transmission (CT) and SWIPT.

A. Modeling of Concurrent RWPT

The limited charging range and efficiency of RWPT, typically constrained to a few meters with relatively low efficiency [10], have motivated the use of multiple power transmitters to concurrently charge wireless sensor nodes [25]. The first models for many-to-one concurrent power transmitting were introduced in [26], where the harvestable energy in both 2D and 3D spaces was determined. However, these models rely on ideal assumptions, such as a single frequency and identical initial transmission phases. To address these limitations, models were extended in [22], considering arbitrary frequency points on the power spectral density curve of narrowband radio waves. Furthermore, the nonlinear superposition of electromagnetic waves during concurrent charging was explored in [24], [27], [28], leading to the development of detailed charging and energy cost models. Moreover, one-to-many models have been developed in [29], [30], where each charger is assumed to serve multiple sensor nodes within its range. These models show that the received energy by each node varies based on its distance from the charger. In many-to-many configurations, the total energy received by a receiver is ideally the sum of all energy contributions from each charger.

While these studies provide foundational models for concurrent RWPT in many-to-one and one-to-many scenarios, they generally assume ideal conditions and lack to account for real-world complexities. For instance, in practical many-to-one deployments, multiple power transmitters are often deployed independently, without tight time synchronization and consistent phase alignment. Additionally, in one-to-many scenarios, interference between neighboring nodes is common. Therefore, our work aims to develop more realistic concurrent RWPT models based on experimental observations, considering the challenges of real-world deployments.

Element	Model	Frequency Range	Power	Gain	Radiation Pattern	Polarization	Efficiency
Power Transmitter	TX91501B	915 MHz (Center)	3W EIRP	8 dBi	H: 60° V: 60°	Vertical	-
Power Transmitter	TX91503	915 MHz (Center)	3W EIRP	6 dBi	H: 70° V: 130°	Horizontal	-
Receiving Antenna	PA-915-01	902 - 928 MHz	-	6.1 dBi	H: 122° V: 68°	Vertical	$< -10 \mathrm{dB}$
Receiving Antenna	DA-915-01	902 - 928 MHz	-	1 dBi	Omni-directional	Vertical	$< -10 \mathrm{dB}$
Receiving Antenna	Rubber Duck	2.4 GHz	-	3 dBi	Omni-directional	Linear	-
Energy Harvesting Board	P2110-EVB	902 - 928 MHz	-12-10 dBm	-	-	-	> 60%
Energy Harvesting Board	P21XXCSR-EVB	GSM and WiFi 2.4 GHz	-15-15 dBm	-	-	-	> 50%
Battery-Free IoT Node	WSN-EVAL-01	2.4 GHz	-	-	-	1	-
Battery IoT Node	Zolertia Z1	2.4 GHz	-	-	-	-	-

B. Experimental Studies on Concurrent RWPT

Extensive research has been conducted on the basic oneto-one RWPT [8]. For instance, [9] demonstrates how environmental factors such as line-of-sight, multipath interference, and material penetration affect the efficiency of wireless power transfer. Despite these efforts, comprehensive experimental studies on concurrent RWPT remain limited. Some progress has been made, such as the development of a distributed antenna system with central control in [16], which utilizes a leader radio with multiple slave radios to generate beamforming power for charging medical implants. Our previous work [12] presented experimental results on concurrent power transmission with omnidirectional and directional receiving antennas. Additionally, the "Octopus Zone" was experimentally demonstrated, where homogeneous zero-energy nodes receive power in a one-to-many concurrent charging. Moreover, the Fresnel diffraction model introduced in [31] for modeling wireless charging in the presence of obstacles has provided valuable insights. This model can be viewed as a case of concurrent power receiving, where obstacles act as "fake receivers" that disrupt the power transfer process.

Overall, these studies show that the presence of homogeneous neighbor nodes and obstacles can significantly affect the received power at a node. In this work, we extend these findings by considering heterogeneous nodes commonly encountered in real-world deployments, such as pure energy-harvesting boards, zero-energy devices operating at different frequencies, and battery-powered IoT devices. Additionally, our study aims to develop accurate and practical models for various charging scenarios to inform effective node deployment and scheduling strategies [7], [32], [33].

C. Concurrent Transmission and SWIPT

Concurrent data transmission [34] in IoT has garnered significant attention as an alternative to traditional access protocols such as TDMA (Time Division Multiple Access) and CSMA (Carrier Sense Multiple Access). CT-based multihop transmission [35] enhances network capacity, reduces latency, and improves reliability in large-scale deployments, particularly in scenarios with constrained connectivity. These benefits make concurrent transmission a compelling strategy for improving throughput and fault tolerance in IoT networks.

Another line of research, Simultaneous Wireless Information and Power Transfer (SWIPT) [19], focuses on transmitting both data and energy within the same wireless signal. SWIPT presents an efficient mechanism for supporting energyautonomous IoT systems by reducing the energy overhead of communication. However, SWIPT inherently involves a trade-off between energy harvesting and information decoding, which requires sophisticated signal processing and receiver design to balance these two objectives. In contrast, our work focuses exclusively on concurrent radiative wireless power transfer, which aims to transmit energy to multiple devices concurrently, without incorporating any form of data communication. Therefore, the models and experiments in this study do not involve the trade-off between energy harvesting and information decoding, as is central to SWIPT. Instead, our focus is on the challenges and performance of multi-source to multi-device energy transfer, including mutual coupling, temporal interference, and power aggregation in concurrent energy transmissions. By isolating the energy transmission component, this study offers novel insights into optimizing power transfer performance in complex many-to-many topologies, which can complement future research that integrates both energy and data transmission in IoT networks.

III. EXPERIMENTAL STUDY

This section presents a comprehensive experimental study on concurrent RWPT. We first introduce the experimental testbed and then detail the experimental setup and results across four fundamental concurrent RWPT situations: one-to-one, many-to-one, one-to-many, and many-to-many scenarios.

A. Experimental Testbed

Fig. 2 illustrates the elements of the testbed used in this study, with key parameters summarized in Table I.

1) Wireless Power Transmitters: The TX91501B Power-caster transmitter operates in the unlicensed 915 MHz ISM band, broadcasting radio waves for RWPT. It uses Direct Sequence Spread Spectrum for power modulation and delivers a power output of 3 watts Effective Isotropic Radiated Power (EIRP). The integrated 8 dBi directional antenna has a beam pattern of 60° width and 60° height, with vertical polarization. Similarly, the PowerSpot TX91503 transmitter operates in the 915 MHz ISM band with a power output of 3 watts EIRP. Its

integrated 6 dBi directional antenna provides a beam pattern of 70° width and 130° height, with horizontal polarization.

- 2) Power Receiving Antennas: These include three types, each with unique characteristics. The patch antenna (PA-915-01) operates within a frequency range of 902-928 MHz, offering a gain of 6.1 dBi and a return loss of less than -10 dB between 908.3 and 920.5 MHz. It features a horizontal radiation pattern with a half-power bandwidth of 122° in the vertical plane and 68° in the horizontal plane, with linear vertical polarization. The dipole antenna (DA-915-01), also covering the 902-928 MHz range, has a gain of 1 dBi and a return loss of less than -10 dB between 894 and 949 MHz. It provides an omnidirectional radiation pattern with a half-power bandwidth of 80° and linear vertical polarization. Additionally, a 2.4 GHz rubber duck antenna was employed to test heterogeneous nodes operating at frequencies distinct from 915 MHz. This omnidirectional antenna offers a nominal gain of 3 dBi and linear polarization, expanding the scope of the experimental setup.
- 3) Energy Harvesting Boards: The boards utilized in this experiment include the P2110-EVB Powerharvester evaluation board and the P21XXCSR-EVB board, each designed for efficient energy harvesting across different frequency ranges. The P2110-EVB evaluation board operates at a center frequency of 915 MHz, with an energy harvesting range of 850–950 MHz. It functions effectively with input power levels as low as 12 dBm and up to 10 dBm, achieving a conversion efficiency exceeding 60%. Meanwhile, the P21XXCSR-EVB board supports six frequency bands, including GSM-850/900/1800/1900 and WiFi 2.4 GHz, accommodating input power ranging from -15 dBm to 15 dBm with a conversion efficiency of over 50%. These boards play a critical role in enabling efficient energy conversion in the experimental testbed.
- 4) IoT Nodes: The IoT nodes deployed in the experimental setup include the WSN-EVAL-01 battery-free wireless sensor node and the Zolertia Z1 Remote node, each serving distinct purposes. The WSN-EVAL-01, part of the Powercast Lifetime Power Energy Harvesting Development Kit [36], transmits essential metrics such as the Received Signal Strength Indicator (RSSI) and the time differential (dT) between packets to the access point. A separate counter records data for each node, and the received data is displayed on a laptop via HyperTerminal. The Zolertia Z1 Remote node, widely used in the research community, was chosen as a battery-powered IoT node to complement the experiment study.
- 5) Metrics: We adopt RSSI and dT as the primary performance metrics in evaluating concurrent RWPT. RSSI reflects the power level of the received signal, serving as a direct indicator of the effectiveness of wireless power transfer at the receiver end. dT, defined as the time elapsed between consecutive power packets, characterizes the temporal dynamics and regularity of power delivery in the network. The choice of these two metrics is motivated by both theoretical and practical considerations. RSSI is widely used in low-power wireless systems to estimate link quality and received power, making it a suitable proxy for energy harvesting performance in the absence of dedicated power sensors. Moreover, in radiative WPT systems where the power is modulated and transmitted in



Fig. 2. Elements of the experimental testbed.

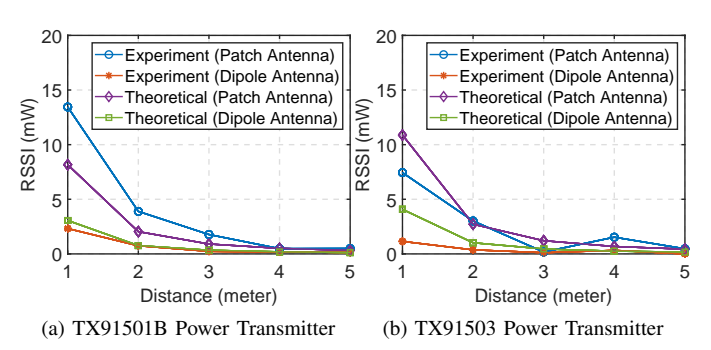


Fig. 3. Results of RSSI in one-to-one concurrent RWPT.

bursts, packet interval provides insight into the temporal consistency and potential interference patterns during concurrent transmission. Together, these metrics capture the spatial and temporal dimensions of power transfer performance, enabling a comprehensive evaluation of multi-device energy delivery under different deployment configurations.

B. One-to-One Concurrent RWPT

We first examined concurrent RWPT in a one-to-one scenario, the simplest configuration where each wireless power transmitter supplies energy to a single battery-free IoT node. This setup is typical in sparse IoBT networks, where either the power transmitters or IoT nodes are separated by significant distances. The evaluation included both the TX91501B and TX91503 power transmitters. The P2110-EVB was selected as the energy harvesting board, equipped separately with a patch antenna and a dipole antenna. The distance between the power transmitter and the receiving node was incrementally increased from 1 meter to 5 meters, in steps of 1 meter.

Fig. 3 presents the experimental results. As expected, the received power decreases exponentially with increasing distance in all setups. Due to its higher directional gain, the patch antenna consistently harvested more power than the dipole antenna. For instance, the power received by the patch antenna from the TX91501B transmitter measured 13.447, 3.892, 1.774, 0.481, and 0.493 mW at distances of 1, 2, 3, 4, and 5 meters, respectively. In contrast, the dipole antenna harvested 2.321, 0.744, 0.235, 0.167, and 0.134 mW under the same conditions. Notably, the power received at 3 meters

from the TX91503 transmitter was significantly lower (0.174 mW for the patch antenna and 0.11 mW for the dipole antenna) compared to the values at 4 meters (1.53 mW) and 5 meters (0.469 mW). This unexpected drop is likely caused by ground-reflected multipath interference, where destructive phase alignment between the direct and reflected signal paths leads to a deep fading effect at specific distances.

Theoretical values were calculated using Powercast's Wireless Power Calculator [37], which is based on the Friis freespace transmission model. Although the calculated values follow the same general trend as the experimental results, a noticeable gap exists between the two. This discrepancy can be attributed to the fact that the theoretical model does not account for real-world factors such as multipath propagation, ground and wall reflections, polarization mismatches, and environmental noise. Additionally, practical limitations in antenna alignment, gain variation, and measurement precision further contribute to these differences. Nonetheless, the experimental and theoretical alignment in trend validates the model's utility and supports its application in evaluating the more complex concurrent RWPT scenarios studied in this work.

C. Many-to-One Concurrent RWPT

We next investigated many-to-one scenarios, which are often employed to enhance power density by increasing the number of power transmitters. As shown in Fig. 4a, we first used one, two, and three homogeneous TX91501B power transmitters to charge a battery-free node equipped with a dipole antenna. The interval between the power transmitters was set to 80 centimeters, with a direct charging distance of 2 meters. A total of 100 packets were recorded for each configuration. The experimental results, including RSSI and packet intervals with smoothing spline fitting curves, are shown in Fig. 5.

The results indicate that increasing the number of power transmitters enhances the performance. While a single power transmitter delivers relatively stable power transfer, multiple transmitters cause fluctuations in received power. Regarding packet intervals, the presence of more power transmitters allows the receivers to charge more rapidly, reducing the time between packets. For example, the average packet intervals for one, two, and three TX91501B power transmitters charging the node with a dipole antenna at 2 meters were 7.3, 4.46, and 2.87 seconds, respectively. The same tests were conducted using a patch antenna in place of the dipole antenna. The results, shown in Fig. 6, exhibited similar trends but with significantly improved performance. For example, the peak received power with three transmitters and a patch receiving antenna increased from 5.4 mW to 20.28 mW, and the packet interval was reduced from 3 seconds to less than 1 second.

We also examined a heterogeneous transmitter setup, where TX91501B and TX91503 power transmitters simultaneously charged a battery-free node, as demonstrated in Fig. 4b. The RSSI and packet interval results for both patch and dipole antenna configurations are shown in Fig. 7. Finally, we studied the impact of orientation on concurrent RWPT in both azimuth and elevation scenarios, as illustrated in Fig. 4c and Fig 4d. In the azimuth configuration, the three TX91501B transmitters



(a) Homogeneous Transmitters

(b) Heterogeneous Transmitters

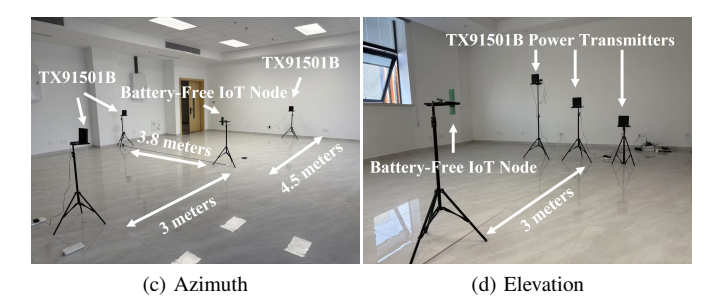


Fig. 4. Experimental setup for many-to-one concurrent RWPT.

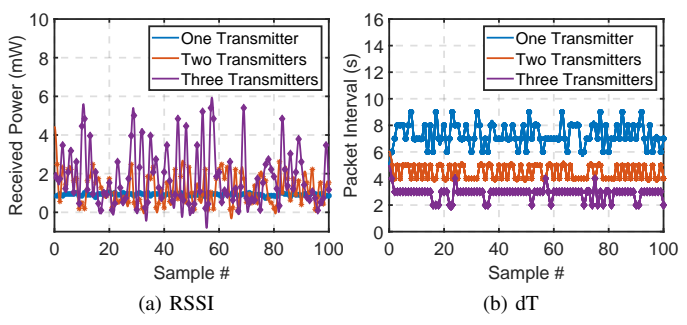


Fig. 5. Many-to-one concurrent RWPT with TX91501B and dipole antenna.

were positioned at distances of 3, 3.8, and 4.5 meters from the IoT node. In the elevation configuration, the transmitters were randomly placed at altitudes of 65 centimeters, 1 meter, and 1.5 meters, with a horizontal distance of 3 meters. The corresponding results, shown in Fig. 7 and Fig. 8, revealed similar trends as in the homogeneous transmitter scenarios, with improvements in power density and fluctuations in received power. However, variations in received power and packet intervals across different transmitter and orientations configurations highlighted the importance of these factors in optimizing the performance of many-to-one concurrent RWPT.

D. One-to-Many Concurrent RWPT

We next explored concurrent RWPT in one-to-many scenarios, a common situation when multiple battery-free IoT nodes are within the charging area of a single wireless power transmitter. We began by evaluating a basic one-to-two concurrent power-receiving configuration, as illustrated in Fig. 9a. The TX91501B served as the wireless power transmitter, positioned at coordinates (0, 75) centimeters. The primary battery-free IoT node, consisting of a P2110-EVB energy harvesting board, a dipole receiving antenna, and a

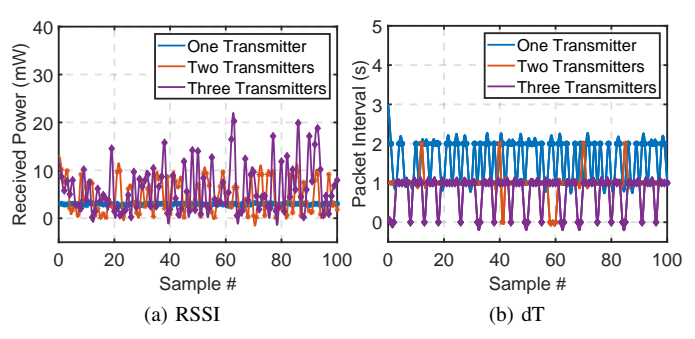
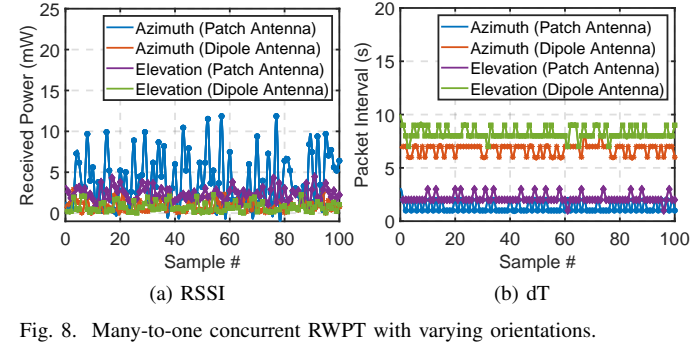


Fig. 6. Many-to-one concurrent RWPT with TX91501B and patch antenna.



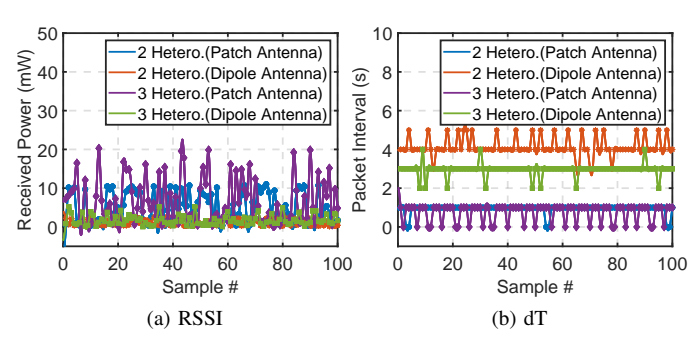
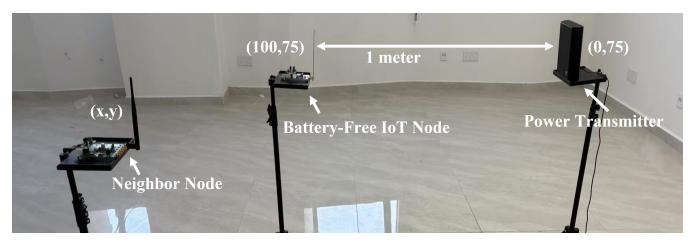


Fig. 7. Many-to-one concurrent RWPT with heterogeneous transmitters.

WSN-EVAL-01 sensor node, was located at (100, 75). A neighboring node was moved in 10-centimeter increments both vertically and horizontally, covering 256 positions (x, y) from (0, 0) to (150, 150). We tested four types of neighboring nodes to represent diverse scenarios in coexisting IoT networks. The first is the same type as the IoT node, which is identical configuration as the primary node. The second is a passive node, which consists of a P2110-EVB energy harvesting board with a dipole antenna but no sensor functionality, emulating a non-active node. The third is a P21XXCSR-EVB energy harvesting board with a rubber duck antenna and WSN-EVAL-01 sensor node, operating at 2.4 GHz. The last is a Zolertia Z1 IoT node powered by a battery.

The results for all four scenarios are presented in Fig. 10. Although the neighboring node's impact on the received power of the primary IoT node is evident in all cases, the initial heatmaps appear blurred due to the limited resolution of the measurement points. After applying cubic spline interpolation in MATLAB, clearer heatmaps for each scenario emerged, as shown in Fig. 11. These heatmaps reveal the "Octopus Zone" energy interference pattern in heterogeneous neighboring IoT nodes. The pattern can be divided into three distinct regions: (1) First Fresnel Zone: received energy decreases due to signal attenuation caused by the neighboring node; (2) Intermediate Zone: follows the Fresnel Zone rule, where signal strength oscillates based on constructive and destructive interference; (3) Shadowing Zone: located behind the primary IoT node, where the neighboring node introduces a wave interference pattern. These observations enabled us to conceptualize a unified theoretical model for one-to-two concurrent RWPT.

We further investigated one-to-four concurrent power-



(a) One-to-Two Concurrent Power Receiving



(b) One-to-Four (Dense Network) (c)

(c) One-to-Four (Sparse Network)

Fig. 9. Experimental setup for one-to-many concurrent RWPT.

receiving scenarios in both dense and sparse network configurations, as illustrated in Fig. 9b and Fig. 9c. The TX91501B was used as the power transmitter. In the dense network, the battery-free IoT node (Rx0) and its three neighboring nodes (Rx1, Rx2, and Rx3) were deployed in close proximity, with 30-centimeter spacing between adjacent nodes. In contrast, the sparse network used a spacing of 2 meters, thereby reducing mutual coupling and near-field effects.

The results, shown in Fig. 12a, demonstrate that increasing the number of neighboring nodes in the dense network introduces significant energy interference, due to superposition and phase cancellation effects from nearby concurrent transmissions. However, this interference does not increase linearly with the number of neighboring nodes. Notably, the 2-Neighbor configuration exhibits the lowest performance, which may seem counterintuitive. This is likely due to unfavorable constructive interference patterns at Rx0 caused by the specific spatial arrangement and phase relationships of the transmitting neighbors. In such a configuration, destructive interference can dominate more than in the other cases, where the additional or less transmitters contribute more diffusely and may partially offset each other's destructive effects. In the sparse network, energy interference in Fig. 12b is significantly reduced, since the larger inter-node distances decrease both coupling and the

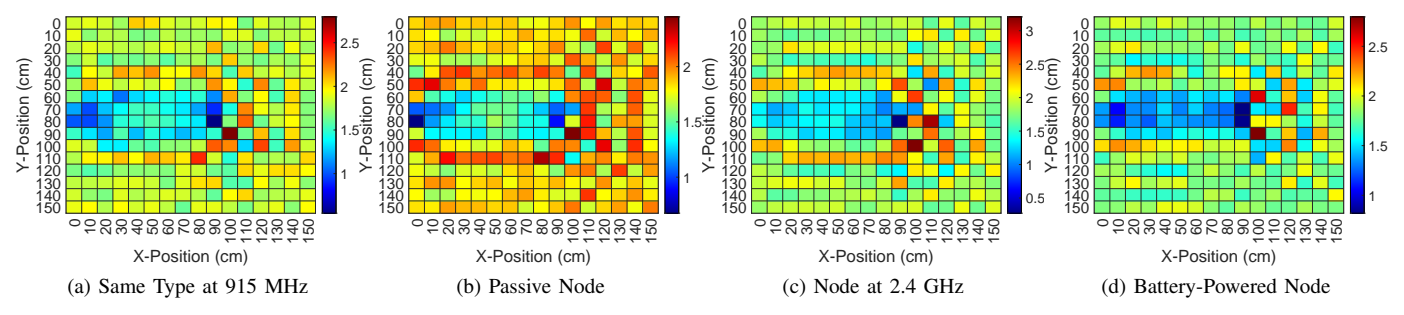


Fig. 10. Received power of a battery-free node during one-to-two concurrent power receiving, with the neighboring node positioned at varying locations.

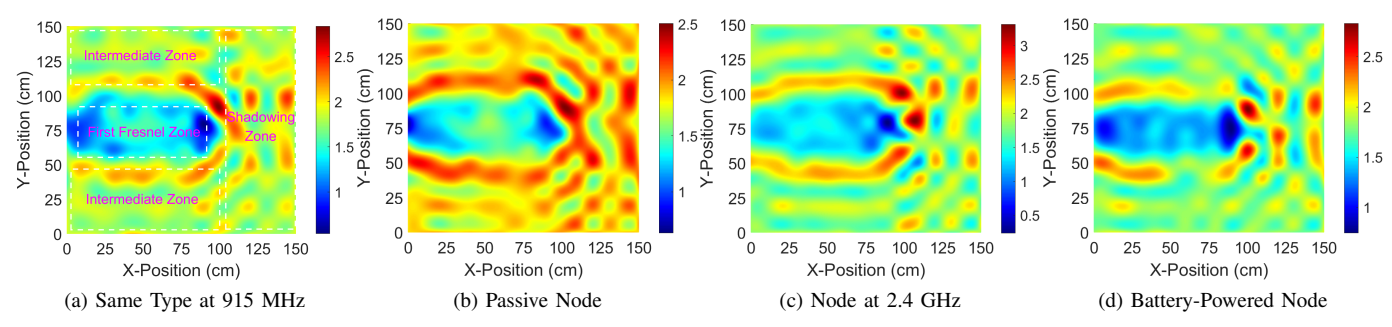


Fig. 11. The corresponding cubic spline interpolation results based on above measurements.

likelihood of strong destructive interference. This allowed us to empirically identify an interference boundary, which will be a critical spatial threshold beyond which the impact of concurrent transmissions becomes negligible.

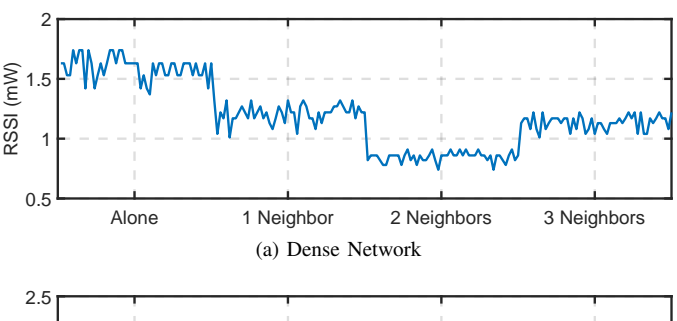
E. Many-to-Many Concurrent RWPT

Finally, we examined many-to-many concurrent RWPT in a paired topology. The experimental setup is depicted in Fig. 13. The wireless power transmitters (TX91501B) were arranged with a 50-centimeter interval, while homogeneous battery-free IoT nodes were placed opposite the transmitters. Each pair maintained a charging distance of 1 meter. The IoT nodes utilized the P2110-EVB energy harvesting board, and we evaluated both patch and dipole antennas.

Fig. 14a and Fig. 14b present the received power data for Node 0 and Node 1, respectively, across 50 samples in 2×2 and 3×2 pair topologies. The results indicate that the peak received power in the 2×2 and 3×2 configurations shows minimal variation. This suggests that the presence of a third power transmitter in the 3×2 topology has a limited impact on the neighboring nodes. This behavior can primarily be attributed to the radiation pattern and polarization characteristics of the wirless power transmitters, which mitigate excessive interference between the pairs. These findings highlight the importance of radiation patter and polarization in many-tomany scenarios, providing valuable insights for designing efficient and interference-resilient power transfer networks.

IV. THEORETICAL MODELING

Based on the experimental observations detailed in the previous section, this part of the study aims to establish



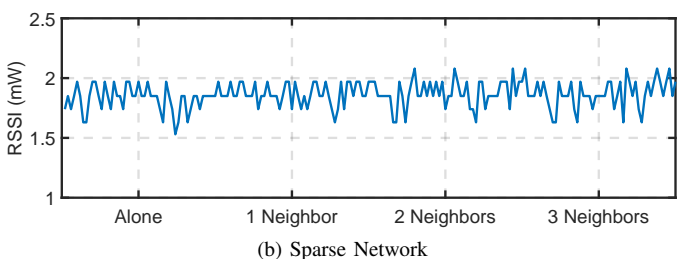


Fig. 12. Experimental results of one-to-four concurrent power receiving.

theoretical models for each of the concurrent RWPT scenarios. These models are developed to provide a mathematical framework for understanding the power transfer dynamics observed experimentally, enabling accurate predictions and optimizations in real-world applications.

A. Network Model

The IoBT network consists of several key components that collaborate to ensure seamless wireless power transfer and communication. These components include wireless power transmitters, battery-free IoT nodes, and base stations.

1) Wireless Power Transmitters: These are responsible for wirelessly transferring power to the battery-free IoT nodes.

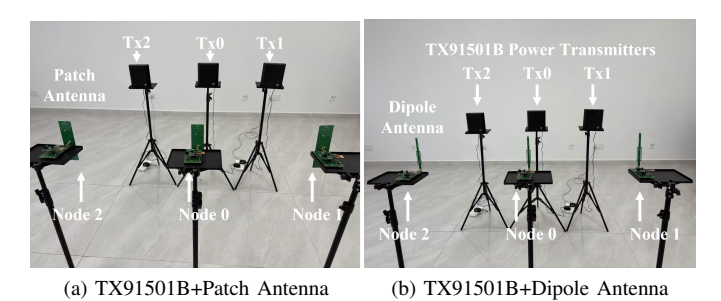
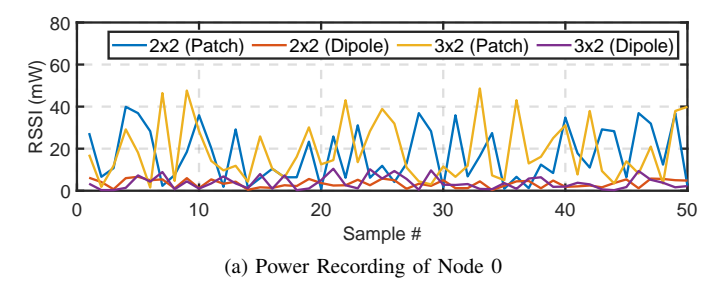


Fig. 13. Experimental setup for many-to-many concurrent RWPT.



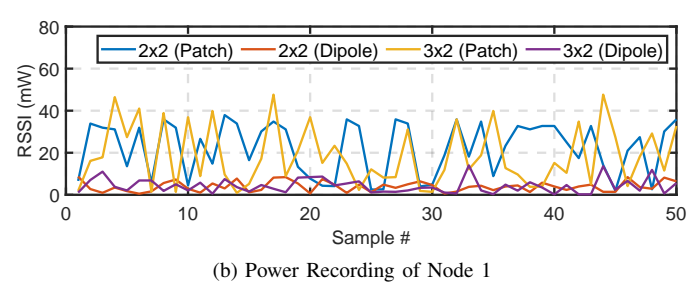


Fig. 14. Experimental results of many-to-many concurrent RWPT.

They are typically powered by renewable energy sources or an electrical grid. In this study, radio frequency (RF) is used for power transfer, although alternative methods such as ultrasound could also be applicable.

- 2) Battery-Free IoT Nodes: These are sustainable smart devices that harvest ambient energy to power their operations. They typically consist of sensors, actuators, and intelligent computing elements, which are capable of sensing environment and responding by actuating certain actions. The nodes are self-sustaining and do not rely on traditional batteries.
- 3) Base Stations (BS): They manage the overall operation of IoBT network by facilitating communication, energy provisioning, and data aggregation. Base stations are responsible for coordinating the wireless power transfer process, monitoring energy levels in both the wireless power transmitters and the IoT nodes, and collecting data from devices in the network.

The network topology for IoBT is distributed and can be represented as a heterogeneous multi-tier architecture, where each component works together to ensure efficient wireless power transfer and communication. The battery-free IoT nodes are deployed across a region or field, which can be modeled in 2D or 3D depending on the application (e.g., environmental monitoring, agricultural IoBT). The coordinates of each device Rx_i are denoted by (x_i, y_i, z_i) , where $i \in [0, N]$ represents the index of the device. The wireless power transmitters are

also distributed within the network and provide power to the IoT nodes. These transmitters can be modeled as a set of points $Tx = \{Tx_0, Tx_1, \ldots, Tx_M\}$, where each transmitter Tx_j is positioned at coordinates (x_j, y_j, z_j) , with $j \in [0, M]$ representing the index of the transmitter.

In this distributed IoBT network, each IoT node may receive power from one or more wireless power transmitters. Devices are assumed to have a limited range for both energy harvesting and communication. The power received by a device depends on several factors, including the distance from the transmitter, the transmission power, and the antenna gain. These components are assumed to communicate with each other using a variety of communication technologies, including Zigbee, LoRa, and backscatter. The network connectivity of the IoBT consists of two main types of links: energy transfer links and communication links. These links are defined by the following:

- 4) Energy Transfer Links: These are the links responsible for transferring power from the wireless power transmitters to the battery-free IoT devices. An energy transfer link exists between a Tx_j and Rx_i if the device is within the energy transfer range of the wireless power transmitter. The energy coverage area depends on the distance, transmission characteristics, and environmental factors.
- 5) Communication Links: These represent the communication paths between each other. An edge (m,n) exists in the communication graph $G=(V_{node},E)$ if the distance between devices m and n is within the communication range $R_{\rm comm}$, and the devices can communicate. Where, V_{node} is the set of battery-free IoT nodes, wireless power transmitters, and base stations. E is the set of communication links, where an edge (m,n) exists if the distance d_{mn} between devices satisfies $d_{mn} \leq R_{\rm comm}$. The distance d_{mn} is calculated using the Euclidean distance formula:

$$d_{mn} = \sqrt{(x_m - x_n)^2 + (y_m - y_n)^2 + (z_m - z_n)^2}$$
 (1)

This graph-based network model allows for efficient energy transfer and communication across the IoBT network. Devices can dynamically adjust their energy harvesting and communication strategies depending on network topology and environment factors, ensuring a scalable and efficient system.

B. One-to-One Concurrent RWPT

Since each pair of wireless power transfer links in one-toone concurrent RWPT operates independently without interference, the model can be established using the Friis Transmission Equation, which is given as follows:

1) Friis Transmission Equation: The received power (P_r) at the battery-free IoT node is given by:

$$P_r = P_t \cdot G_t \cdot G_r \cdot \left(\frac{\lambda}{4\pi d}\right)^2 \tag{2}$$

where, P_t represents the transmitted power, G_t is the gain of the transmitting antenna, and G_r is the gain of the receiving antenna. The wavelength of the transmission signal is denoted as λ , which is given by $\lambda = \frac{c}{f}$, where c is the speed of light and f is the frequency. Finally, d is the distance between the wireless power transmitter and the battery-free IoT node.

Based on the experimental observations, ground reflection introduces an additional propagation path for the signal. The signal that is reflected from the ground can combine with the direct line-of-sight signal, potentially enhancing or degrading the received power depending on the relative phase and distance. For simplicity, we assume that the reflection path is the most significant, and the other potential reflections (e.g., from buildings or other surfaces) can be neglected. Thus, the received signal power can be modeled as the sum of the direct path and the reflected path, taking into account the relative distance and phase shift due to the reflection. The total received power is modified by the reflection coefficient and path difference. It can be expressed as:

$$P_r = P_t \cdot G_t \cdot G_r \cdot \left(\frac{\lambda}{4\pi d}\right)^2 \left(1 + \Gamma \cdot \frac{R_{\text{ref}}}{R_{\text{dir}}}\right) \tag{3}$$

where, the reflection coefficient Γ , which depends on the angle of incidence and the material properties of the ground, modifies the received power due to ground reflection. $R_{\rm ref}$ and $R_{\rm dir}$ denote the distances of the reflected and direct paths. The term $\left(1+\Gamma\cdot\frac{R_{\rm ref}}{R_{\rm dir}}\right)$ accounts for the constructive or destructive interference due to the reflected signal.

2) Capacitor Charging Model: The capacitor in the battery-free node stores the energy being transferred, and its charge/discharge behavior determines how the energy accumulates over time. In this case, the charging time depends on both the power received from wireless power transmitter and the charging characteristics of the capacitor. The energy stored in the capacitor, denoted by $E_{\rm cap}$, is given by the equation:

$$E_{\rm cap} = \frac{1}{2}CV^2 \tag{4}$$

where, C is the capacitance of the receiver's energy storage, and V is the voltage across the capacitor. The voltage across the capacitor over time t is described by:

$$C\frac{dV(t)}{dt} = I_{charging} = \frac{P_r}{V(t)}$$
 (5)

Solving this, we get:

$$V(t) = \sqrt{V_0^2 + \frac{2P_r}{C}t}$$
 (6)

where, V_0 is the initial voltage across the capacitor.

3) Charging Time Calculation: The charging time T_c is the time it takes for the voltage to reach a final voltage $V_{\rm final}$. Based on above capacitor charging model, the energy stored in the capacitor is:

$$E_{\text{final}} = \frac{1}{2}CV_{\text{final}}^2 \tag{7}$$

Thus, the charging time T_c is given by:

$$T_c = \frac{C}{2P_r} \left(V_{\text{final}}^2 - V_0^2 \right) \tag{8}$$

C. Many-to-One Concurrent RWPT

In the presence of multiple transmitters, the received power is not simply the sum of the individual received powers, because the electromagnetic waves can interfere with each other. The interference can either be constructive (signals reinforce each other) or destructive (signals cancel each other out). This depends on the relative phase of the signals from each wireless power transmitter at the location of the battery-free IoT node. The total received power P_r at the device is determined by the vector sum of the electric field contributions from all transmitters, which depend on the phase shift and distance between the transmitter and the receiver.

1) Vector Sum of Power Signals: Let's consider the complex form of the received signal from each transmitter, incorporating both amplitude and phase information:

$$E_j = \sqrt{P_r^{(j)}} e^{i\phi_j} = \sqrt{P_r^{(j)}} \left(\cos(\phi_j) + i\sin(\phi_j)\right)$$
 (9)

where, E_j is the electric field from the j-th transmitter, $P_r(j)$ is the received power from the j-th transmitter, given by the Friis equation, and ϕ_j is the phase shift of the j-th transmitter's signal, which depends on the distance between the wireless power transmitter and battery-free IoT node.

Thus, the total electric field E_{total} at the device is the vector sum of the electric fields from each transmitter:

$$E_{\text{total}} = \sum_{j=0}^{M} E_j = \sum_{j=0}^{M} \sqrt{P_r^{(j)}} e^{i\phi_j}$$
 (10)

The total received power at the device is proportional to the squared magnitude of the total electric field:

$$P_r = |E_{\text{total}}|^2 = |\sum_{j=0}^{M} \sqrt{P_r^{(j)}} e^{i\phi_j}|^2$$
 (11)

or represented by:

$$P_r = \left(\sum_{j=0}^{M} \sqrt{P_r^{(j)}} \cos(\phi_j)\right)^2 + \left(\sum_{j=0}^{M} \sqrt{P_r^{(j)}} \sin(\phi_j)\right)^2$$
(12)

2) Phase Shift and Interference Modeling: The phase shift ϕ depends on the relative position of the wireless power transmitter and the battery-free IoT node. Let's define the position of the IoT node as (x_0, y_0, z_0) and the position of the j-th wireless power transmitter as (x_j, y_j, z_j) . The distance between the wireless power transmitter j and the battery-free IoT node is d_{0j} , and the phase shift is given by:

$$\phi_{0j} = 2\pi \left(\frac{d_{0j}}{\lambda} + \Delta \phi_{0j} \right) \tag{13}$$

where, λ is the wavelength of the transmitted signal, d_{0j} is the distance between the wireless power transmitter Tx_j and the battery-free IoT node Rx_0 . $\Delta\phi_{0j}$ is the initial phase of the transmitter, which may vary randomly.

Using the expression for the total electric field, the total received power P_r can be rewritten as:

$$P_r = \left| \sum_{j=0}^{M} \sqrt{\frac{P_t G_t G_r \lambda^2}{(4\pi d_{0j})^2}} e^{i\left(\frac{2\pi d_{0j}}{\lambda} + \Delta\phi_{0j}\right)} \right|^2 \tag{14}$$

This equation accounts for both amplitude attenuation (Equation (2)) and phase shifts of the different transmitters. If reflection path is also considered, Equation (3) should be used.

3) Average Power in Random Transmitter Distribution: When the wireless power transmitters are randomly distributed, the distances d_{0j} and the initial phases $\Delta\phi_{0j}$ are random variables. Therefore, we must average over all possible configurations of the transmitters.

To simplify this, we typically assume a Poisson distribution for the number of transmitters in a given area and integrate over the distribution of distances and phase shifts. In terms of distance distribution, the distance d_{0j} between the receiver and each distributed transmitter follows a certain distribution depending on the area. For example, in a uniform distribution over a 2D plane, the distance d_{0j} has a known probability distribution. The average distance can be computed using this distribution. As for phase distribution, the initial phase $\Delta\phi_{0j}$ for each transmitter is typically assumed to be uniformly distributed in the range $[0,2\pi]$, since the random positioning of transmitters leads to a random phase shift. The expected total received power is the average of the total received power expression over all random positions and phase shifts:

$$\mathbb{E}[P_r] = \mathbb{E}\left[\left| \sum_{j=0}^{M} \sqrt{\frac{P_t G_t G_r \lambda^2}{(4\pi d_{0j})^2}} e^{i\left(\frac{2\pi d_{0j}}{\lambda} + \Delta\phi_{0j}\right)} \right|^2 \right]$$
(15)

Given the random nature of both d_{0j} and $\Delta\phi_{0j}$, computing the expected received power in practical scenarios, especially with a large number of wireless power transmitters, often relies on Monte Carlo simulations. This approach involves randomly distributing transmitters within the region of interest, computing the received power based on the corresponding distances and phase offsets for each realization, and repeating the process many times. By averaging the results across numerous iterations, the simulation captures the aggregate effect of constructive and destructive interference, providing a statistically robust estimate of the received power.

D. One-to-Many Concurrent RWPT

In the scenario of one-to-many concurrent RWPT, where multiple neighbor IoT nodes exist, the received power at a receiver Rx_0 from a transmitter Tx_0 is influenced by the presence of neighboring interference nodes. These nodes can be situated in various regions relative to Rx_0 and Tx_0 , namely the First Fresnel Zone (Blocking Zone), Intermediate Zone (Fresnel Zone), and the Shadowing Zone (Interference Zone). Let us define the three regions and the corresponding models:

1) First Fresnel Zone (Blocking Effect): In the First Fresnel Zone, each interference node Rx_i (where i denotes the node index) can partially or completely block the line-of-sight (LoS) path between the wireless power transmitter and a battery-free IoT node, causing attenuation in the received power. The received power at Rx_0 from Tx_0 in this region is:

$$P_r^{FirstFresnel} = \frac{P_t G_t G_r \lambda^2}{(4\pi d_0)^2} (1 - \beta_i)$$
 (16)

where, P_t is the transmitted power, G_t and G_r are the antenna gains of Tx_0 and Rx_0 , respectively, and λ is the wavelength. d_0 is the distance between Tx_0 and Rx_0 . The attenuation

factor due to the blocking effect of interference node Rx_i , denoted as β_i , is defined such that $0 \le \beta_i \le 1$. The value of β_i depends on the size and material of the obstruction. Specifically, $\beta_i = 0$ indicates no blockage, meaning the LoS path is clear, and $\beta_i = 1$ indicates complete blockage, where the LoS path is fully obstructed by the node.

2) Intermediate Zone (Fresnel Zone): In the Intermediate Zone, the received power at Rx_0 exhibits oscillations due to constructive and destructive interference between the direct path from Tx_0 and Rx_0 , and the reflected paths influenced by the interference nodes. The received power in this region is:

$$P_r^{Intermediate} = \frac{P_t G_t G_r \lambda^2}{(4\pi d_0)^2} \left(1 + \gamma_i \cos\left(2\pi \frac{d_i}{\lambda} + \phi_i\right) \right)$$
(17)

where, d_i is the distance between Rx_i and Rx_0 . The interference factor γ_i represents the strength of the interference, where $0 \le \gamma_i \le 1$. It depends on the distance and alignment of the interfering node relative to Tx_0 and Rx_0 . Specifically, $\gamma_i = 0$ indicates no oscillatory interference from the node, while $\gamma_i = 1$ indicates maximum interference oscillations from the node. The phase shift ϕ_i is given by $\phi_i = \left(\frac{2\pi d}{\lambda} + \pi\right)$, where d is the distance between the wireless power transmitter and the interference node. It is important to note that when an electromagnetic wave, such as a radio or microwave signal, reflects off a conducting surface (e.g., a metal object, antenna, or surface with high impedance), the reflected wave undergoes a phase inversion. This means that the phase of the reflected signal shifts by 180° relative to the incident signal, which is a standard physical property of wave behavior at boundaries where a wave transitions from a medium of lower impedance to one of higher impedance.

3) Shadowing Zone (Interference Behind Rx_0): In the Shadowing Zone, when the interference node Rx_i is located behind Rx_0 relative to Tx_0 , diffraction and scattering effects lead to fluctuations in the received power. The received power in this region is:

$$P_r^{Shadowing} = \frac{P_t G_t G_r \lambda^2}{(4\pi d_0)^2} \left(1 + \delta_i \cos\left(2\pi \frac{d_i}{\lambda} + \phi_i\right) \right)$$
(18)

where, $0 \le \delta_i \le 1$ represents the interference caused by diffraction and scattering effects when Rx_i is behind Rx_0 . The value of δ_i depends on the geometry and material causing diffraction and scattering. Specifically, $\delta_i = 0$ indicates no diffraction or scattering interference from the node, while $\delta_i = 1$ represents maximum diffraction or scattering interference from the node.

4) Total Received Power at Rx_0 Considering All Regions: To compute the total received power at Rx_0 from all the interference nodes, we sum the contributions from the three regions. Here, we consider the primary inference signal from each neighboring node to Rx_0 . The effects of multiple scattering, reflection, and higher-order interference are not included in this model. Thus, the total received power at R_x is:

$$P_r = P_r^{FirstFresnel} + P_r^{Intermediate} + P_r^{Shadowing}$$

$$= \frac{P_t G_t G_r \lambda^2}{(4\pi d_0)^2} \sum_{i=0}^{N} \left[(1 - \beta_i) + \gamma_i \cos\left(2\pi \frac{d_i}{\lambda} + \phi_i\right) \right]$$

$$+ \delta_i \cos\left(2\pi \frac{d_i}{\lambda} + \phi_i\right)$$
(19)

where, the sum runs over all interference nodes, with N being the total number of interference nodes. The terms $(1-\beta_i)$, γ_i , and δ_i account for the blocking effect, interference oscillations in the intermediate zone, and diffraction/scattering effects in the shadowing zone, respectively. If higher-order effects were included, the model would need to be expanded to account for additional interference signals, resulting from scattering and reflections before reaching the target node.

E. Many-to-Many Concurrent RWPT

Lastly, in the scenario of many-to-many concurrent RWPT, multiple wireless power transmitters and multiple IoT nodes are simultaneously transmitting and receiving power (or only reflect the power signal), respectively.

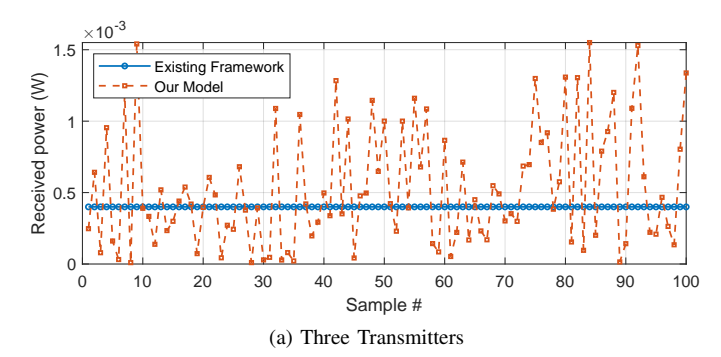
Let M+1 be the number of transmitters and N+1 be the number of receivers. Thus, the received power at Rx_0 from all transmitters is the sum of the power contributions from each, taking into account the interference between neighbor IoT nodes. By integrating the many-to-one model (Equation (14)) and the one-to-many model (Equation (19)), we derive the many-to-many concurrent RWPT model. The approach involves using Equation (14) to represent the ideal received power from a single wireless power transmitter in the Equation (19). The resulting expression is as follows:

$$P_r = \left| \sum_{j=0}^{M} \sqrt{\frac{P_t G_t G_r \lambda^2}{(4\pi d_{0j})^2}} e^{i\left(\frac{2\pi d_{0j}}{\lambda} + \Delta\phi_{0j}\right)} \right|^2 \cdot \sum_{i=0}^{N} \left[(1 - \beta_{ij}) + \gamma_{ij} \cos\left(2\pi \frac{d_{0i}}{\lambda} + \phi_{ij}\right) + \delta_{ij} \cos\left(2\pi \frac{d_{0i}}{\lambda} + \phi_{ij}\right) \right]$$
(20)

where, d_{0j} represents the distance between Rx_0 and transmitter Tx_j . d_{0i} represents the distance between Rx_0 and Rx_i . β_{ij} is the attenuation factor due to the blocking effect of an interference node Rx_i at the transmitter Tx_j . γ_{ij} denotes the interference strength from another nearby node, which depends on the distance and alignment between the transmitter Tx_j and receiver Rx_i . δ_{ij} captures the interference caused by diffraction and scattering effects. Finally, ϕ_{ij} represents the phase term for the transmitter-receiver pair (Rx_i, Tx_j) , which determines how signals from different transmitters interact at receiver Rx_i .

V. MODEL VALIDATION

In this section, we present simulation results to validate the theoretical models developed in this study for concurrent RWPT. The simulations are conducted using MATLAB, with key parameter settings aligned with those listed in Table I.



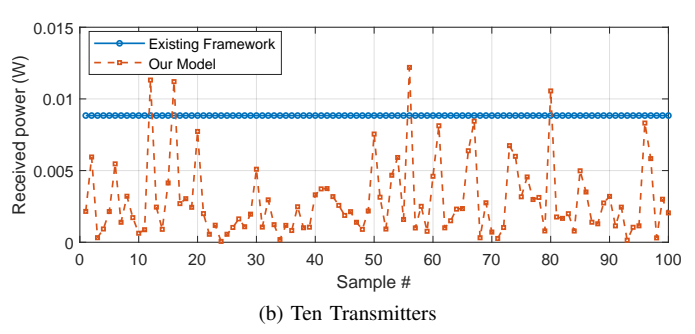


Fig. 15. Simulation results of many-to-one concurrent RWPT.

Since the one-to-one RWPT model has been validated both experimentally and theoretically in Sec. III-B, this section focuses on the remaining three cases.

A. Many-to-One Concurrent RWPT

Simulation Settings. To evaluate the performance of the many-to-one concurrent RWPT model, simulations were conducted under two distinct conditions: one representing existing frameworks, where transmitter phases are idealistically fixed due to the lack of consideration for network synchronization issues, and our model reflecting realistic distributed RWPT networks, where synchronization imperfections cause transmitter phases to vary over time. In the simulations, we considered scenarios with three and ten transmitters. Each transmitter was randomly positioned with distances uniformly distributed between 2 to 5 meters from the receiver. The initial phase offset for each transmitter was uniformly distributed within $[0,2\pi]$. For the fixed-phase scenario, these initial phases were kept constant across all simulation trials, while in the realistic scenario, the phases varied independently for each trial.

Results. As shown in Fig. 15, the simulation results highlight significant performance differences between the idealized fixed-phase model and our proposed model with time-varying transmitter phases. In the scenario with three transmitters, the fixed-phase model produced a stable received power of 0.3999 mW, with virtually no variance. In contrast, the realistic model incorporating synchronization imperfections resulted in a higher mean received power of 0.5212 mW, albeit with notable variability (standard deviation: 0.4161 mW). When scaled to ten transmitters, these effects became more pronounced. The idealized model yielded a mean power of 8.838 mW with zero variance, indicative of consistent constructive interference. However, under the realistic time-varying phase

model, the mean power dropped to 2.896 mW, accompanied by substantial variability (standard deviation: 2.643 mW).

Lessons Learned. These results demonstrate that the fixed-phase assumption significantly overestimates received power and fails to capture realistic performance dynamics in distributed RWPT systems. The introduction of transmitter phase variation, caused by synchronization imperfections, leads to greater power variability and a generally reduced mean power in larger-scale systems. Importantly, the behavior observed in the simulations closely matches trends seen in experimental data (e.g., Fig. 5), providing strong validation for our analytical model. These findings underscore the critical need to account for realistic synchronization conditions when designing and evaluating RWPT systems. Ignoring such factors could result in misleadingly optimistic performance expectations, particularly in systems with many transmitters.

B. One-to-Many Concurrent RWPT

Simulation Settings. To evaluate the proposed one-to-many concurrent RWPT model, we designed a 2D simulation environment based on the physical setup of real-world experiments. The primary wireless power transmitter was placed at coordinates (0 cm, 75 cm). The primary battery-free IoT receiver node was fixed at (100 cm, 75 cm). An interfering node, representing a neighboring passive or semi-active node capable of reflecting or absorbing RF energy, was moved in 10 cm increments across a 2D plane spanning from (0 cm, 0 cm) to (150 cm, 150 cm), forming a 16×16 grid (256 positions).

Results. The resulting power distribution heatmaps in Fig. 16 demonstrates a spatially varying interference pattern. The received power at the primary node exhibits constructive and destructive interference fringes. These patterns closely match experimentally observed results (i.e., Fig. 10 and Fig. 11), validating the effectiveness of our model. While the overall spatial structure and interference trends closely match the experimental measurements, slight mismatches in absolute received power levels are observed. These discrepancies can arise from uncertainties or simplifications in modeling hardware characteristics such as transmitter output power fluctuations, reflection and scattering complexity, or antenna gain patterns. To address these mismatches, fine-tuning factors such as a global calibration multiplier can be incorporated. These tuning parameters allow alignment of the simulation output with experimental data, enabling a more accurate prediction of received power without altering the core structure of the physical model. Once calibrated, the simulation framework can generalize well across similar deployment scenarios.

Lessons Learned. In contrast to our model, existing frameworks typically assume independent energy reception for each node in the network. Under these models, the presence or movement of neighboring nodes does not affect the received power at a given node, resulting in a homogeneous and oversimplified power field. This assumption introduces a substantial discrepancy from real-world behavior, where RF interference, reflections, and local signal obstructions have a profound impact on energy harvesting performance. By modeling the inter-node coupling effects, our approach demon-

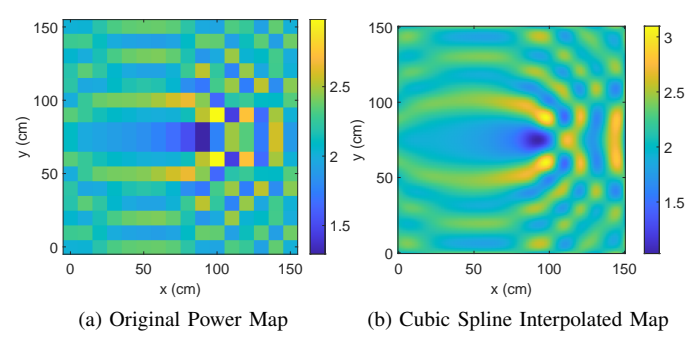


Fig. 16. Simulation results of one-to-two concurrent power receiving, with the neghboring node positioned at varying locations.

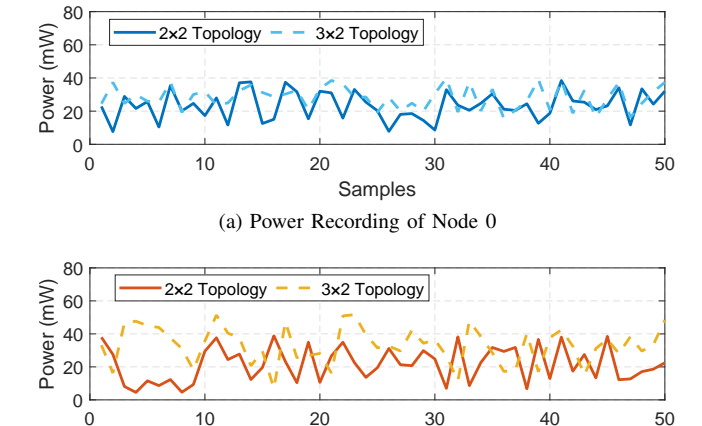


Fig. 17. Simulation results of many-to-many concurrent RWPT.

strates the nonlinear and location-sensitive dynamics of oneto-many concurrent RWPT. This highlights the critical need for interference-aware energy models in designing and optimizing real-time wireless power delivery systems for dense batteryfree IoT deployments.

Samples

(b) Power Recording of Node 1

C. Many-to-Many Concurrent RWPT

Simulation Settings. Finally, we examine the many-tomany concurrent RWPT model using a paired topology. We consider two representative topologies: a 2×2 setup with two transmitters and two receivers, and a 3×2 setup where a third transmitter is added while maintaining the same receiver positions. All transmitters are placed with a horizontal spacing of 50 cm, while each transmitter-receiver pair maintains a vertical charging distance of 1 meter. The wireless power transmitters are modeled after the TX91501B devices operating at 915 MHz with an EIRP of 3 W. The receivers mimic P2110-EVB energy harvesting boards. To evaluate time-varying effects caused by phase interference and signal composition, we simulate received power at each receiver across 50 timedomain samples. The received power is computed in milliwatts (mW), considering the contributions from all transmitters based on the many-to-many model described in Equation (20).

Results. Fig. 14a and Fig. 14b show the received power for Node 0 and Node 1, respectively, in both 2×2 and 3×2 configurations. The results demonstrate relatively stable power

levels across all 50 samples, with no significant variation between the two configurations. The presence of the third transmitter in the 3×2 setup introduces minor fluctuations but does not substantially increase the peak power at either receiver. This matches the experimental observations, where the additional transmitter in the 3×2 arrangement produced minimal impact on adjacent receivers due to the spatial separation and directional radiation of the energy beams. Additionally, the simulated time-domain curves successfully replicate the observed power ripple caused by random phase interference, thereby validating the realism and accuracy of the proposed simulation model.

Lessons Learned. Most conventional RWPT frameworks analyze one-to-one or one-to-many transmission patterns, neglecting the mutual coupling and temporal interference that emerge in many-to-many systems. These models often assume isolated charging links and fail to capture the collective effects of simultaneous multi-beam radiation. Our proposed model addresses this critical gap by integrating both transmitterside superposition and receiver-side interference, including blocking, scattering, and polarization effects. By capturing the temporal dynamics induced by concurrent transmissions and random phase shifts, our model provides deeper insight into power fluctuation patterns that would otherwise be overlooked. The results further highlight the importance of considering beam alignment and antenna characteristics when designing scalable and interference-resilient wireless power networks.

VI. CONCLUSION AND FUTURE WORK

This study aimed to provide a comprehensive understanding of concurrent RWPT for the IoBT. The experimental findings highlight how various scenarios impact received power and packet interval performance across all four concurrent RWPT scenarios. The key takeaways and lessons learned are summarized as follows:

- 1) One-to-One Concurrent RWPT: In this fundamental scenario, where multiple wireless power transmitters and IoT nodes do not interfere with each other, the experimental results confirmed that the *Friis transmission equation* predicted received power. However, ground reflection effects significantly impacted accuracy, suggesting the need for a correction factor to account for the environment's physical properties. This insight is critical for designing scalable IoBT systems that rely on precise power transfer predictions.
- 2) Many-to-One Concurrent RWPT: Contrary to the assumption of simple additive power transfer or perfect synchronization in previous studies, our experiments demonstrated that the received power fluctuates considerably due to asynchronous energy transfer in the distributed network. Notably, both homogeneous and heterogeneous power transmitters increased power density but also introduced significant fluctuations, underlining the importance of optimizing transmitter orientation. These findings challenge previous models and provide a basis for refining power transfer strategies in large-scale IoBT networks.
- 3) One-to-Many Concurrent RWPT: Different from existing studies that assume IoT nodes are unaffected by neighboring devices, our experiments revealed that dense network

conditions led to complex interference between neighboring IoT nodes. This interference was observed to either enhance the received power by up to 1.7 times or degrade it to as low as 31% of the original power. Interestingly, even nodes operating on different frequencies or power types contributed to this interference. In contrast, sparse networks exhibited reduced interference, suggesting that defining an *interference boundary* is essential for optimal power management. These results shed new light on network density's role in the IoBT.

- 4) Many-to-Many Concurrent RWPT: Where multiple transmitter-receiver pairs are involved, our study found that increasing the pairs had minimal variation in performance. This stability is attributed to the *radiation patterns and polarization characteristics* of the transmitters and receivers, which remain relatively unaffected by the increased number of pairs.
- 5) Unified Theoretical Models: Building upon experimental results, the study introduces unified theoretical models and validation for concurrent RWPT, providing a step-by-step approach that includes practical formulas and guidelines for each scenario. These models offer a robust framework for future research and development in real-world IoBT systems.

The empirical results and validated theoretical models presented in this study offer a fresh perspective on concurrent RWPT, laying a solid foundation for future research. Key directions include developing adaptive power scheduling algorithms for dynamic network conditions, optimizing transmitter trajectories to improve energy coverage and reduce interference in large-scale and mobile IoBT networks, and devising strategies for optimal placement of IoT nodes and transmitters to enhance energy efficiency and minimize interference. Additionally, adaptive techniques to manage interference in dense networks, such as frequency management, beamforming, and polarization, are crucial. Moreover, extending the models to assess scalability and their impact on large-scale IoBT deployments, including system performance, reliability, and energy security, will further advance the field.

It is important to note that practical RF energy harvesting circuits exhibit nonlinear behavior, particularly saturation when the input power exceeds a certain threshold. However, our theoretical models are based on the linear Friis transmission equation, which assumes ideal conditions and focuses on the propagation and power distribution characteristics in space. This simplification allows us to isolate and analyze spatial and interference effects in concurrent transmission scenarios without introducing hardware-specific nonlinearities. While saturation effects are indeed relevant in high-input regimes, the experimental measurements in our study were conducted under low to moderate power levels, where the harvesting circuits operate largely within their linear region. Incorporating saturation behavior into the theoretical framework would require detailed modeling of specific rectifier characteristics, which can vary across hardware implementations and is therefore left as future work for device-specific optimization.

ACKNOWLEDGMENT

This work is supported by the Marie Skłodowska-Curie Actions (MSCA) Postdoctoral Fellowship MILESTONE-6G (Grant No. 101201988).

REFERENCES

- [1] G. Moloudian, M. Hosseinifard, S. Kumar, R. B. V. B. Simorangkir, J. L. Buckley, C. Song, G. Fantoni, and B. O'Flynn, "Rf energy harvesting techniques for battery-less wireless sensing, industry 4.0, and internet of things: A review," *IEEE Sensors Journal*, vol. 24, no. 5, pp. 5732–5745, 2024.
- [2] D. Ma, G. Lan, M. Hassan, W. Hu, and S. K. Das, "Sensing, computing, and communications for energy harvesting iots: A survey," *IEEE Communications Surveys Tutorials*, vol. 22, no. 2, pp. 1222–1250, 2020.
- [3] T. Jiang, Y. Zhang, W. Ma, M. Peng, Y. Peng, M. Feng, and G. Liu, "Backscatter communication meets practical internet of things: A survey and outlook," *IEEE Communications Surveys and Tutorials*, vol. 25, no. 3, pp. 2021–2051, 2023.
- [4] S. Roy, A. N. M. W. Azad, S. Baidya, M. K. Alam, and F. Khan, "Powering solutions for biomedical sensors and implants inside the human body: A comprehensive review on energy harvesting units, energy storage, and wireless power transfer techniques," *IEEE Transactions on Power Electronics*, vol. 37, no. 10, pp. 12 237–12 263, 2022.
- [5] S. Naser, L. Bariah, S. Muhaidat, and E. Basar, "Zero-energy devices empowered 6g networks: Opportunities, key technologies, and challenges," *IEEE Internet of Things Magazine*, vol. 6, no. 3, pp. 44–50, 2023.
- [6] S. Ahmed, B. Islam, K. S. Yildirim, M. Zimmerling, P. Pawełczak, M. H. Alizai, B. Lucia, L. Mottola, J. Sorber, and J. Hester, "The Internet of Batteryless Things," *Communications of the ACM*, vol. 67, no. 3, p. 64–73, feb 2024.
- [7] Z. Cai, Q. Chen, T. Shi, T. Zhu, K. Chen, and Y. Li, "Battery-free wireless sensor networks: A comprehensive survey," *IEEE Internet of Things Journal*, vol. 10, no. 6, pp. 5543–5570, 2023.
- [8] Y. Liu, D. Li, B. Du, L. Shu, and G. Han, "Rethinking sustainable sensing in agricultural internet of things: From power supply perspective," *IEEE Wireless Communications*, vol. 29, no. 4, pp. 102–109, 2022.
- [9] Y. Liu, D. Li, H. Dai, C. Li, and R. Zhang, "Understanding the impact of environmental conditions on zero-power internet of things: An experimental evaluation," *IEEE Wireless Communications*, vol. 30, no. 6, pp. 152–159, 2023.
- [10] V. Palazzi, R. Correia, X. Gu, S. Hemour, K. Wu, A. Costanzo, D. Masotti, E. Fazzini, A. Georgiadis, H. Kazemi, R. Pereira, N. Shinohara, D. Schreurs, J.-C. Chiao, A. Takacs, D. Dragomirescu, and N. B. Carvalho, "Radiative wireless power transfer: Where we are and where we want to go," *IEEE Microwave Magazine*, vol. 24, no. 2, pp. 57–79, 2023.
- [11] X. Gu, S. Hemour, and K. Wu, "Far-field wireless power harvesting: Nonlinear modeling, rectenna design, and emerging applications," *Proceedings of the IEEE*, vol. 110, no. 1, pp. 56–73, 2022.
- [12] Y. Liu, D. Li, H. Dai, X. Ma, and C. A. Boano, "Understanding concurrent radiative wireless power transfer in the iot: Out of myth, into reality," *IEEE Wireless Communications*, vol. 31, no. 3, pp. 398–405, 2024.
- [13] A. Jaiswal, S. Shivateja, A. Hazra, N. Mazumdar, J. Singh, and V. G. Menon, "Uav-enabled mobile ran and rf-energy transfer protocol for enabling sustainable iot in energy-constrained networks," *IEEE Transactions on Green Communications and Networking*, vol. 8, no. 3, pp. 1118–1127, 2024.
- [14] H. Guo, R. Wu, Y. Ma, S. Sun, Y. Wang, B. Qi, J. Gao, and C. Xu, "Synergy-payoff-maximization-based rechargeable adaptive energy-efficient dual-mode data gathering using renewable energy sources," *IEEE Internet of Things Journal*, vol. 11, no. 21, pp. 35292–35305, 2024.
- [15] J. Du, M. Xu, S. S. Gill, and H. Wu, "Computation energy efficiency maximization for intelligent reflective surface-aided wireless powered mobile edge computing," *IEEE Transactions on Sustainable Computing*, vol. 9, no. 3, pp. 371–385, 2024.
- [16] X. Fan, L. Shangguan, R. Howard, Y. Zhang, Y. Peng, J. Xiong, Y. Ma, and X.-Y. Li, "Towards flexible wireless charging for medical implants using distributed antenna system," in *Proceedings of the 26th Annual International Conference on Mobile Computing and Networking*, ser. MobiCom '20. New York, NY, USA: Association for Computing Machinery, 2020.
- [17] Y. Zhang and C. You, "SWIPT in Mixed Near- and Far-Field Channels: Joint Beam Scheduling and Power Allocation," *IEEE Journal on Selected Areas in Communications*, vol. 42, no. 6, pp. 1583–1597, 2024.
- [18] H. Yang, X. Yuan, J. Fang, and Y.-C. Liang, "Reconfigurable intelligent surface aided constant-envelope wireless power transfer," *IEEE Trans*actions on Signal Processing, vol. 69, pp. 1347–1361, 2021.

- [19] C. Psomas, K. Ntougias, N. Shanin, D. Xu, K. Mayer, N. M. Tran, L. Cottatellucci, K. W. Choi, D. I. Kim, R. Schober, and I. Krikidis, "Wireless information and energy transfer in the era of 6g communications," *Proceedings of the IEEE*, vol. 112, no. 7, pp. 764–804, 2024.
- [20] M. A. Halimi, T. Khan, Nasimuddin, A. A. Kishk, and Y. M. Antar, "Rectifier circuits for rf energy harvesting and wireless power transfer applications: A comprehensive review based on operating conditions," *IEEE Microwave Magazine*, vol. 24, no. 1, pp. 46–61, 2023.
- [21] D. Sarkar, T. Khan, F. A. Talukdar, and S. R. Rengarajan, "Computational intelligence for modeling and optimization of rfeh and wpt systems: A comprehensive survey," *IEEE Microwave Magazine*, vol. 24, no. 9, pp. 46–60, 2023.
- [22] P. Guo, X. Liu, S. Tang, and J. Cao, "Concurrently wireless charging sensor networks with efficient scheduling," *IEEE Transactions on Mobile Computing*, vol. 16, no. 9, pp. 2450–2463, 2017.
- [23] Z. Ma, S. Zhang, J. Wu, Z. Qian, Y. Zhao, and S. Lu, "Fast charging scheduling under the nonlinear superposition model with adjustable phases," ACM Transactions on Sensor Networks, vol. 15, no. 4, Sep. 2019.
- [24] T. Liu, Y. Ma, M. Ren, J. Yang, J. Peng, J. Yang, and D. Wu, "Concurrent charging with wave interference for multiple chargers," *IEEE/ACM Transactions on Networking*, vol. 32, no. 3, pp. 2525–2538, 2024.
- [25] M. Ren, H. Dai, T. Liu, X. Deng, W. Dou, Y. Yang, and G. Chen, "Understanding wireless charger networks: Concepts, current research, and future directions," *IEEE Communications Surveys & Tutorials*, pp. 1–1, 2024.
- [26] M. Y. Naderi, K. R. Chowdhury, and S. Basagni, "Wireless sensor networks with rf energy harvesting: Energy models and analysis," in 2015 IEEE Wireless Communications and Networking Conference (WCNC), 2015, pp. 1494–1499.
- [27] C. Lin, Z. Yang, J. Ren, L. Wang, W. Zhong, G. Wu, and Q. Zhang, "Are you really charging me?" in 2022 IEEE 42nd International Conference on Distributed Computing Systems (ICDCS), 2022, pp. 724–734.
- [28] Y. Ma, D. Wu, M. Ren, J. Peng, J. Yang, and T. Liu, "Concurrent charging with wave interference," in *IEEE INFOCOM 2023 - IEEE Conference on Computer Communications*, 2023, pp. 1–10.
- [29] C. Lin, W. Yang, H. Dai, T. Li, Y. Wang, L. Wang, G. Wu, and Q. Zhang, "Near optimal charging schedule for 3-d wireless rechargeable sensor networks," *IEEE Transactions on Mobile Computing*, vol. 22, no. 6, pp. 3525–3540, 2023.
- [30] H. Dai, Y. Zhang, W. Wang, R. Gu, Y. Qu, C. Lin, L. Xu, J. Zheng, W. Dou, and G. Chen, "Placing wireless chargers with multiple antennas," *IEEE Transactions on Mobile Computing*, vol. 23, no. 6, pp. 7517–7536, 2024.
- [31] C. Lin, S. Hao, H. Dai, W. Yang, L. Wang, G. Wu, and Q. Zhang, "Maximizing charging efficiency with fresnel zones," *IEEE Transactions on Mobile Computing*, vol. 23, no. 1, pp. 612–629, 2024.
- [32] W. Yang, C. Lin, H. Dai, J. Ren, L. Wang, G. Wu, and Q. Zhang, "Precise wireless charging in complicated environments," *IEEE/ACM Transactions on Networking*, pp. 1–16, 2024.
- [33] A. Kumar and J. Singh, "Optimizing location and power of chargers to reduce interference in battery-less wsns," *IEEE Sensors Journal*, vol. 24, no. 16, pp. 26552–26563, 2024.
- [34] M. Zimmerling, L. Mottola, and S. Santini, "Synchronous transmissions in low-power wireless: A survey of communication protocols and network services," ACM Computing Surveys, vol. 53, no. 6, Dec. 2020.
- [35] M. Baddeley, C. A. Boano, A. Escobar-Molero, Y. Liu, X. Ma, V. Marot, U. Raza, K. Römer, M. Schuss, and A. Stanoev, "Understanding concurrent transmissions: The impact of carrier frequency offset and rf interference on physical layer performance," ACM Transactions on Sensor Networks, vol. 20, no. 1, Oct. 2023.
- [36] Powercast, https://www.powercastco.com, accessed: 2024-11-29.
- [37] P. W. P. Calculator, https://calculator.powercastco.com, accessed: 2024-11-29.



Ye Liu (Senior Member, IEEE) received the M.S. and Ph.D. degrees in electronic science and engineering from Southeast University, Nanjing, China, in 2013 and 2018, respectively. He was a Visiting Scholar with Montana State University, Bozeman, MT, USA, from 2014 to 2015. He was a visiting Ph.D. student with the Networked Embedded Systems Group, RISE Swedish Institute of Computer Science, Kista, Sweden, from 2017 to 2018. He was a Macau Young Scholar with the Macau University of Science and Technology, Macau, SAR, China,

from 2022 to 2024. His research interests include Internet of Things, wireless power transfer, energy harvesting, and tiny machine learning. He is a Co-Director for IEEE MMTC Review, an Associate Editor for IEEE Access, IJSNET, and IJSN, and a Guest Editor for IEEE Network and IEEE TCE.



Honggang Wang (Fellow, IEEE) is the founding Chair and Professor of the Department of Graduate Computer Science and Engineering, Katz School of Science and Health, Yeshiva University in New York City. He was a Professor at UMass Dartmouth (UMassD). He is an alumnus of NAE Frontiers of Engineering program. He graduated 30 MS/Ph.D. students and produced high-quality publications in prestigious journals and conferences in his research areas, winning several prestigious best paper awards. His research interests include Internet of Things

and its applications in health and transportation (e.g., autonomous vehicles) domains, Machine Learning and Big Data, Multimedia and Cyber Security, Smart and Connected Health, Wireless Networks, and Multimedia Communications. He is an IEEE distinguished lecturer and a Fellow of AAIA. He has served as the Editor in Chief (EiC) for IEEE Internet of Things Journal during 2020–2022. He was the past Chair (2018–2020) of IEEE Multimedia Communications Technical Committee and the past IEEE eHealth Technical Committee Chair (2020–2021).



Mikael Gidlund (Senior Member, IEEE) received the Licentiate of Engineering degree in radio communication systems from the KTH Royal Institute of Technology, Stockholm, Sweden, in 2004, and the Ph.D. degree in electrical engineering from Mid Sweden University, Sundsvall, Sweden, in 2005. From 2008 to 2015, he was a Senior Principal Scientist and Global Research Area Coordinator of Wireless Technologies with ABB Corporate Research, Västeräs, Sweden. From 2007 to 2008, he was a Project Manager and a Senior Specialist with Nera

Networks AS, Bergen, Norway. From 2006 to 2007, he was a Research Engineer and a Project Manager with Acreo AB, Hudiksvall, Sweden. Since 2015, he has been a Professor of Computer Engineering at Mid Sweden University. He holds more than 20 patents (granted and pending) in the area of wireless communication. His current research interests include wireless communication and networks, wireless sensor networks, access protocols, and security. Dr. Gidlund is an Associate Editor of the IEEE Transactions on Industrial Informatics.